8920 *Biochemistry* **2009,** *48,* 8920–8928
DOI: 10.1021/bi9011258

BIOCHEMISTRY
including biophysical chemistry & molecular biology
Article

Isocyanides Inhibit Human Heme Oxygenases at the Verdoheme Stage[†]

John P. Evans, Sylvie Kandel, and Paul R. Ortiz de Montellano*

Department of Pharmaceutical Chemistry, University of California, 600 16th Street, San Francisco, California 94158-2517

Received July 2, 2009; Revised Manuscript Received August 19, 2009

ABSTRACT: Heme oxygenases (HO) catalyze the oxidative cleavage of heme to generate biliverdin, CO, and free iron. In humans, heme oxygenase-1 (hHO-1) is overexpressed in tumor tissues, where it helps to protect cancer cells from anticancer agents, while HOs in fungal pathogens, such as *Candida albicans*, function as the primary means of iron acquisition. Thus, HO can be considered a potential therapeutic target for certain diseases. In this study, we have examined the equilibrium binding of three isocyanides, isopropyl, *n*-butyl, and benzyl, to the two major human HO isoforms (hHO-1 and hHO-2), *Candida albicans* HO (CaHmx1), and human cytochrome P450 CYP3A4 using electronic absorption spectroscopy. Isocyanides coordinate to both ferric and ferrous HO-bound heme, with tighter binding by the more hydrophobic isocyanides and 200−300-fold tighter binding to the ferrous form. Benzyl isocyanide was the strongest ligand to ferrous heme in all the enzymes. Because the dissociation constants (K_D) of the ligands for ferrous heme−hHO-1 were below the limit of accuracy for equilibrium titrations, stopped-flow kinetic experiments were used to measure the binding parameters of the isocyanides to ferrous hHO-1. Steady-state activity assays showed that benzyl isocyanide was the most potent uncompetitive inhibitor with respect to heme with a K_I = 0.15 μM for hHO-1. Importantly, single turnover assays revealed that the reaction was completely stopped by coordination of the isocyanide to the verdoheme intermediate rather than to the ferric heme complex. Much tighter binding of the inhibitor to the verdoheme intermediate differentiates it from inhibition of, for example, CYP3A4 and offers a possible route to more selective inhibitor design.

Heme oxygenase plays a key role in heme degradation by catalyzing the regiospecific oxidation of iron protoporphyrin IX, producing biliverdin IXα, CO, and free ferrous iron. In humans, biliverdin reductase (BVR[1]) subsequently reduces biliverdin IXα to bilirubin, which after conjugation with glucuronic acid is readily excreted. The two organic products, bilirubin and CO, have potent antioxidative, anti-inflammatory, and antiapoptotic properties (*1*). CO is increasingly viewed as an essential neurotransmitter akin to nitric oxide (*2*), and HO is the only endogenous source of this molecule. Two major isoforms of heme oxygenase exist within the human: (a) hHO-1, which is induced by a number of stimuli including heat shock, heavy metals, hemin, UV irradiation, oxidative stress, and other toxins, including chemotherapeutics, primarily within the spleen and liver, and (b) hHO-2, which is constitutively expressed over a wide organ distribution but at higher concentrations in the brain and testis. In part because of their different tissue localization, hHO-1 is primarily responsible for heme homeostasis, whereas hHO-2 is involved in the neuronal effects of carbon monoxide (*3*). The notion of targeting hHO-1 for induction to achieve pharmacologic and therapeutic benefits, especially against diseases such as atherosclerosis, has therapeutic promise (*4*). However, in the case of cancer, hHO-1 is one of the most potent antioxidative defenses in tumor cells and protects aberrant cells from therapies aimed at their destruction (*5*). In addition, heme has been shown to be the preferred source of iron for *Staphylococcus aureus* during the initial stages of infection (*6*), and some bacterial and fungal pathogens are capable of utilizing heme as their sole iron source. Therefore, the development of potent and selective HO inhibitors is a promising route to novel anticancer, antibacterial, and antifungal therapeutic approaches.

Human heme oxygenase inhibitors have been primarily pursued for their suppression of neonatal jaundice, a common condition in newborns caused by inefficient bilirubin elimination (*7*). Most, such as Sn or Zn protoporphyrin IX, are metalloporphyrin-based with structural similarities to heme. However, these inhibitors suffer from photoreactivity and are nonspecific for HO, also inhibiting enzymes such as nitric oxide synthase (NOS) and soluble guanylate cyclase (sGC), particularly when used at high concentrations (*8*). The addition of poly(ethylene glycol) conjugates of zinc protoporphyrin make it more water-soluble and more selective for HO (*9*). Other compounds based on azalanstat, an imidazole-dioxolane, have been found to inhibit hHO-1 and hHO-2 (*10*), and it has been shown that different degrees of selectivity can be achieved in the inhibition of HO-1 over HO-2 by modifying this lead framework (*11*). Structural studies reveal that these compounds inhibit HO activity by competing with O_2 for binding to the distal site of the heme iron (*12*, *13*). Their binding is facilitated by the large hydrophobic cavity adjacent to the heme pocket, which is strategically located at the α−meso edge to function as a CO-trapping site (*14*). The goal of this study was to investigate

[†]This research was supported by grant DK30297 from the National Institutes of Health.

*To whom correspondence should be addressed. Phone: +1 415-476-2903. Fax: +1 415-502-4728. E-mail: ortiz@cgl.ucsf.edu.

[1]Abbreviations: BSA, bovine serum albumin; BVR, biliverdin reductase; CaHmx1, *Candida albicans* heme oxygenase; CPR, NADPH-cytochrome P450 reductase; DMSO, dimethyl sulfoxide; EDTA, ethylenediaminetetraacetic acid; HO, heme oxygenase; hHO, human heme oxygenase; K_D, dissociation constant; NADPH, nicotinamide adenine dinucleotide phosphate; NOS, nitric oxide synthase; SD, standard deviation; sGC, soluble guanylate cyclase.

 Published on Web 08/20/2009

the potential utility of the isocyanide function in the generation of HO inhibitors.

Isocyanide compounds are generally water-soluble and can be considerably bulkier than O_2 or CO yet mimic the way in which these gaseous molecules coordinate to heme. Isocyanides of varying sizes have been used as sensitive probes for assessing the steric accessibility of the ligand binding site to the heme iron in hemoproteins. A number of previous studies have focused on isocyanide coordination to hemoglobin (*15*), myoglobin (*16*), NOS (*17*), and cytochrome P450 (*18*). As would be expected from an O_2/CO mimic, the Fe(II)−isocyanide complexes are characterized by much stronger binding than the Fe(III) complexes. Of the hemoproteins examined prior to this study, the ferrous cytochrome P450 exhibited the strongest isocyanide binding (K_D < 10 μM) with bulkier functional groups binding more favorably.

Here we report the use of a series of three isocyanides, isopropyl, *n*-butyl, and benzyl, to probe the active sites of the two major human heme oxygenase isoforms (hHO-1 and hHO-2). Using electronic absorption spectroscopy, we also compared the binding affinities for two additional enzymes. One, the heme oxygenase from *Candida albicans* (CaHmx1), an opportunistic pathogen in humans, is essential for iron uptake (*19*). Human cytochrome P450 CYP3A4, which is of major importance due to its high abundance in the human liver, broad substrate specificity, and frequent involvement in clinically relevant drug−drug interactions (*20*, *21*), was examined as a reference against which to compare HO inhibition. We found that isocyanides with more hydrophobic substituents bind more tightly to hHO-1, hHO-2, CaHmx1, and CYP3A4, especially to the ferrous form. However, we characterized the mechanism of inhibition for the human heme oxygenases more fully and, surprisingly, have determined that the specific catalytic step most effectively inhibited was that of verdoheme degradation, not the initial heme oxidation that the equilibrium binding parameters characterize. This demonstrates that selective inhibition of heme oxygenases over other hemoproteins by an inhibitor with isocyanide functionality may be feasible.

EXPERIMENTAL PROCEDURES

Chemicals. Nicotinamide adenine dinucleotide phosphate (NADPH), bovine serum albumin (BSA), hemin chloride, ethylenediaminetetraacetic acid (EDTA), dimethyl sulfoxide (DMSO), sodium dithionite, hydrogen peroxide (H_2O_2), ampicillin, glucose, isopropyl isocyanide, *n*-butyl isocyanide, and benzyl isocyanide were purchased from Sigma-Aldrich (St. Louis, MO). Isocyanide stock solutions (1 M) were made up in DMSO, and working stocks (1 mM) were constructed in 0.1 M phosphate, pH 7.4 (standard buffer). The concentration of the stock solution of H_2O_2 was determined from ε_{240} = 43.6 M^{-1} cm^{-1} (*22*). Other chemicals were of the highest grade commercially available.

Enzymes. Truncated hHO-1 lacking the 23 C-terminal residues was expressed and purified according to published procedures (*23*). Rat biliverdin reductase (*24*), human NADPH-cytochrome P450 reductase (CPR) (*25*), CaHmx1 (*26*), and CYP3A4 (*27*) were expressed in *E. coli* and purified to apparent homogeneity as described elsewhere. Lysozyme, glucose oxidase, and catalase were purchased from Sigma-Aldrich (St. Louis, MO).

Expression and Purification of hHO-2. Truncated hHO-2 lacking the 23 C-terminal residues in the pBAce expression vector construct was transformed into *E. coli* DH5α. Plates with fresh colonies were used to inoculate 6 mL of Luria−Bertani medium containing 100 μg/mL ampicillin. From the fresh midlog phase cultures, 3 mL was used to inoculate 1.5 L cultures of the same media. The cells were grown at 37 °C for 18 h. The harvested cells were lysed by sonication in 100 mM potassium phosphate buffer (pH 7.8) containing 2 mM EDTA, 2 mM phenylmethylsulfonyl fluoride, a Roche protease inhibitor tablet, and lysozyme. The soluble proteins were separated by ultracentrifugation at 100000*g* for 45 min (4 °C). The resulting supernatant was passed through a 100 mL S-Sepharose column (Sigma-Aldrich, St. Louis, MO) directly onto a 100 mL Q-Sepharose column (Sigma-Aldrich, St. Louis, MO), both pre-equilibrated with 50 mM potassium phosphate buffer (pH 7.4) containing 1 mM EDTA. The Q-Sepharose column was washed with 50 mM potassium phosphate buffer (pH 7.4, 1 mM EDTA) and eluted with a 600 mL linear gradient going from 50 mM potassium phosphate (pH 7.4, 1 mM EDTA) to 50 mM potassium phosphate (pH 7.4, 1 mM EDTA, 400 mM NaCl). The pure fractions of hHO-2 were combined, brought to 1.5 M NaCl, and applied to a 60 mL phenyl Sepharose 6 fast flow column (GE Healthcare, Piscataway, NJ) pre-equilibrated with 500 mL of 50 mM potassium phosphate (pH 7.4), 1.5 M NaCl, washed with the same buffer and eluted with 50 mM potassium phosphate (pH 7.4). The fractions showing pure apo-hHO-2 were combined, concentrated, and converted in 100 mM potassium phosphate (pH 7.4) by multiple cycles of concentration and dilution. Reconstitution with heme was performed as previously described (*23*).

Equilibrium Ligand Binding Titrations. Binding of isocyanides to ferric and ferrous heme−hHO-1, hHO-2, CaHmx1, and CYP3A4 complexes was monitored by UV−visible spectroscopy using a Varian Cary 50 UV−visible spectrophotometer at 20 °C. Ferric heme titrations were performed aerobically while ferrous heme titrations were performed in the presence of trace amounts of sodium dithionite under strictly anaerobic conditions within a glovebox. Successive 1 μL aliquots of isocyanide were added to a cuvette containing 2−5 μM protein in standard buffer (800 μL). Alterations in the heme spectra as a function of ligand concentration were used to determine the thermodynamic dissociation constant (K_D) by fitting to a hyperbolic curve (eq 1).

$$\Delta\mathrm{Abs} = \frac{\mathrm{Abs}_{max} L}{L + K_D} \quad (1)$$

where ΔAbs is the change in signal due to formation of the *Ligand·Enzyme* complex, Abs_{max} is the amplitude of the titration, and L is the concentration of ligand. In the cases where the enzyme concentration E was within 5-fold of the apparent K_D value, the data were fit to the quadratic eq 2.

$$\Delta\mathrm{Abs} = \frac{\mathrm{Abs}_{max}}{2E}\left[(K_D + E + L) - \sqrt{(K_D + E + L)^2 - (4E \cdot L)}\right] \quad (2)$$

In the case of CYP3A4, the data were best fit to the equation describing a two site model (eq 3), where K_1 and K_2 describe the equilibrium dissociation constants for the high affinity and low affinity sites, respectively.

$$\Delta\mathrm{Abs} = \frac{\mathrm{Abs}_{1_{max}} L}{L + K_1} + \frac{\mathrm{Abs}_{2_{max}} L}{L + K_2} \quad (3)$$

Binding of the isocyanides to ferric verdoheme−hHO-1 was performed by adding increasing concentrations of isocyanide to

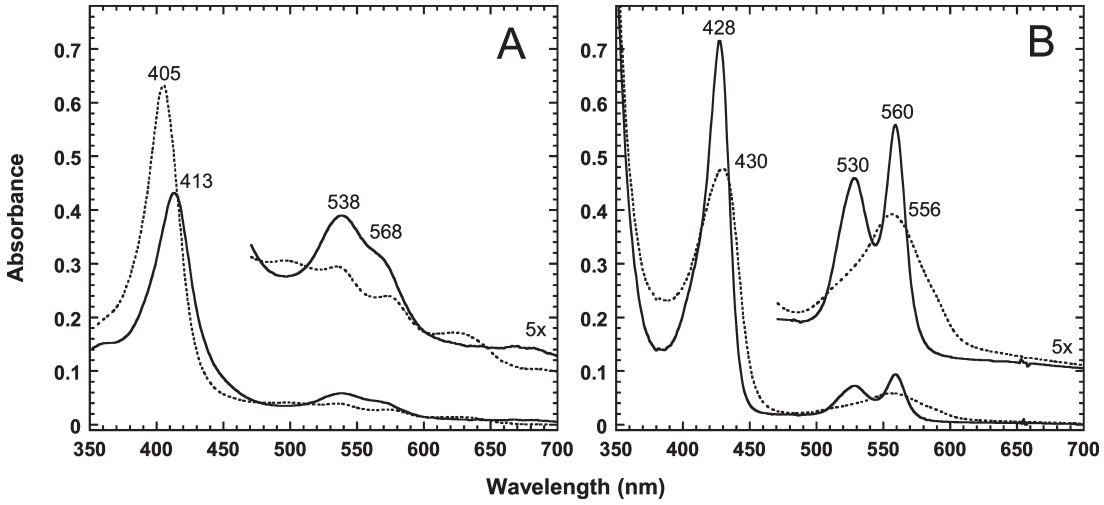

FIGURE 1: Equilibrium binding of *n*-butyl isocyanide to heme−hHO-1. Shown are the absorbance spectra monitored by UV−visible spectroscopy of the ferric (A) and ferrous (B) heme−hHO-1 in the presence (solid line) and absence (dotted line) of 25 μM *n*-butyl isocyanide.

freshly prepared verdoheme−hHO-1, generated from the reaction of 4 μM ferric heme−hHO-1 with 1 equiv of H_2O_2 (*28*). Formation of verdoheme was monitored by UV−visible spectroscopy, reaching a maximum after 20 min. At this point, the ligand, diluted in DMSO, was added and the effects on the heme spectra were recorded. Difference spectra were obtained by subtracting the resting enzyme spectrum without isocyanide (addition of DMSO) from that containing isocyanide. Dissociation constants (K_D) were determined in duplicate or triplicate from the hyperbolic plots of the respective differences in the 404−424 nm trough-to-peak absorbance versus the ligand concentration.

Stopped-Flow Kinetic Measurements. The association and dissociation reactions of the series of isocyanides with hHO-1 were measured at 20 °C on a Hi-Tech Scientific SF-61 DX2 double mixing stopped-flow system equipped with a KinetaScan diode array detector. The stopped-flow was made anaerobic by flushing the system with anaerobic standard buffer containing 1 mM sodium dithionite, followed by a large volume of anaerobic standard buffer alone. All solutions were prepared in an anaerobic glovebox and placed in gastight syringes (Hamilton) sealed with rubber septa. The data were analyzed using Specfit and were fit to the single-exponential equation as described in the text.

All kinetic association measurements were carried out in anaerobic standard buffer containing 1 mM sodium dithionite. The final concentration of hHO-1 was 2.5 μM. Ligand binding rates were measured at various final isocyanide concentrations, ranging from 25 to 200 μM.

The kinetic dissociation measurements were carried out in anaerobic standard buffer containing 2 Units/mL glucose oxidase, 10 mM glucose, and 10 μg/mL catalase. The stock solution of nitric oxide was prepared by equilibrating the buffer with 1 atm of the pure NO at room temperature. The solubility of NO gas under 1 atm at 20 °C was ~1.8 mM. The final concentrations in the stopping syringe were 2.5 μM hHO-1, 5 μM isocyanide, 12.5 μM sodium dithionite, and approximately 900 μM NO.

Heme Oxygenase Steady State Activity Assays. hHO-1 and hHO-2 activities were determined by the rate of bilirubin formation at 468 nm using a Spectramax UV−visible plate reader (Molecular Devices, Sunnyvale, CA) according to previously described conditions with minor modifications (*29*, *30*). Reaction mixtures (200 μL) consisted of 0.2 μM HO, 1 μM CPR, 4 μM BVR, 15 μM hemin, 0.1 M phosphate supplemented with 10 mg/mL BSA, pH 7.4. The reactions were incubated at 37 °C for 1 min prior to the addition of 400 μM NADPH to initiate the reaction. The initial rate of bilirubin formation was calculated using an extinction coefficient of 43.5 mM^{-1} cm^{-1}. Isocyanide concentrations were varied from 0.02 to 11 μM. To determine the IC_{50} values, the percentage of control activity was fitted to the following equation by nonlinear regression using the program KaleidaGraph (Abelbeck/Synergy Software, Reading, PA): $p = p\text{max} + \{(p\text{min} - p\text{max})/[1 + (I/IC_{50})^n]\}$, where p (percentage of control activity) is the relative amount of remaining enzyme activity due to the inhibitor concentration I, n is the Hill coefficient, $p\text{max} \leq 100$, and $p\text{min} \geq 0$.

Single-Turnover Reactions. The reaction mixtures (500 μL) contained 5 μM heme−hHO-1 or heme−hHO-2 complexes, 40 nM CPR, and 25 μM NADPH in standard buffer in the presence and absence of varying concentrations of isocyanide. Spectra were recorded at 15 s intervals over the range of 300−800 nm for 20 min on a Varian Cary 50 UV−visible spectrophotometer at room temperature.

RESULTS

Equilibrium Binding of Isocyanides to Ferric Heme Complexes. Isocyanides bind to the iron of heme in the same manner as carbon monoxide (*16*). The affinities of the three isocyanides for the resting heme complexes of a series of four enzymes, hHO-1, hHO-2, CaHmx1, and CYP3A4, were evaluated spectrophotometrically by monitoring the heme spectral changes upon the addition of ligand. Addition of increasing concentrations of isocyanide to the ferric heme complexes of hHO-1, hHO-2, CaHmx1, and CYP3A4 resulted in a decrease and red-shift in the corresponding Soret absorption maximum. For instance, upon isocyanide binding to the ferric resting state of heme-hHO-1, the six-coordinate high-spin spectrum with a Soret maximum at 405 nm shifts to a spectrum with a Soret maximum at 413 nm and bands at 538 and 568 nm (Figure 1A), a spectrum similar to that of the six-coordinate low-spin spectrum of hHO-1 at alkaline pH (*31*). These differences were utilized to perform titrations and obtain spectral dissociation constants (K_D). Difference spectra generated by subtracting the resting enzyme without isocyanide from that containing bound isocyanide produced a binding saturation curve and the fitted K_D values (Table 1).

Table 1: Equilibrium Binding Parameters of Isopropyl, *n*-Butyl, and Benzyl Isocyanide for the Ferric and Ferrous Heme Complexes of hHO-1, hHO-2, CaHmx1, and CYP3A4 in 0.1 M Phosphate Buffer (pH 7.4), 20 °C[a]

	K_D (μM)						
	Fe(III)				Fe(II)		
isocyanide	hHO-1	hHO-2	CaHmx1	CYP3A4	hHO-1	CaHmx1	CYP3A4
isopropyl	250 ± 30	170 ± 10	3800 ± 500[c]	13 ± 3 840 ± 40	0.54 ± 0.08	4.3 ± 0.4	3.7 ± 0.6[b]
n-butyl	29 ± 3	33 ± 3	ND	25 ± 9 240 ± 50	0.07 ± 0.03[b]	0.5 ± 0.1[b]	1.3 ± 0.5
benzyl	6 ± 1	8 ± 1	ND	14 ± 3 92 ± 8	0.03 ± 0.01[c]	0.03 ± 0.01[c]	0.40 ± 0.09[b]

[a]Values are presented as group means ± standard deviation (SD). ND = not determined. [b]Values are the average of two replicates with the corresponding propagated error. [c]Values presented for a single experiment with the error calculated from the line of best fit.

It is apparent from the K_D constants (Table 1) determined from these absorbance titrations that the size of the functional group attached to the isocyanide greatly affects the affinity of the isocyanides for the heme oxygenases. The binding affinity of isopropyl isocyanide was the weakest, whereas the higher molecular weight *n*-butyl isocyanide displayed a 9-fold higher affinity for hHO-1, while the K_D value for benzyl isocyanide was even lower with an almost 42-fold greater affinity. hHO-2 displayed a similar trend, only with a greater affinity for isopropyl isocyanide. These large changes in affinity reflect the sensitivity of the active site to the bulkier functional groups, which can be readily accommodated by the hydrophobic cavity of the human heme oxygenases.

CYP3A4 required a fitting of the spectral equilibrium binding data to a two binding site model that yielded both a low- and a high-affinity component. This is expected considering the crystal structures reveal a large active site with the capacity to bind multiple ligand molecules (*32*, *33*). The low-affinity site showed a similar trend to the aforementioned enzymes, favoring bulkier alkyl substituted isocyanides, with the weakest affinity for isopropyl isocyanide and the strongest affinity for benzyl isocyanide but still over 15-fold weaker than hHO-1. Although there was no trend between the isocyanides at the high-affinity site, they were all, within error, of 16 μM.

Whereas equilibrium binding of the isocyanides to ferric human heme oxygenases and CYP3A4 was rapid, binding to ferric CaHmx1 was much slower. The resting heme complex of CaHmx1 at pH 7.4 did not exhibit the six-coordinate high-spin spectrum typical of the human heme oxygenases. Instead, the ferric heme resting state was six-coordinate low-spin, with a Soret absorbance at 411 nm; furthermore, this ligand was not titratable (*26*). Titration with isopropyl isocyanide caused very small changes to the absorbance spectrum of CaHmx1 without reaching full saturation up to 7 mM but allowed for an estimate of the K_D = 3.8 mM. Addition of *n*-butyl isocyanide caused little change to the Soret in the presence of up to 6 mM ligand, at the limit of its solubility in aqueous solutions; however, at this concentration, there were more significant but very gradual changes in the spectrum due to binding of the ligand observed over a period of 60 min. The fastest binding was observed with benzyl isocyanide, where binding was observed upon the addition of 1 mM benzyl isocyanide by the increase in absorbance at 430 nm over the course of 30 min (Figure 2). Because of the slow rates of ligand binding, it was not possible to measure accurate K_D values for ferric CaHmx1 using equilibrium binding studies.

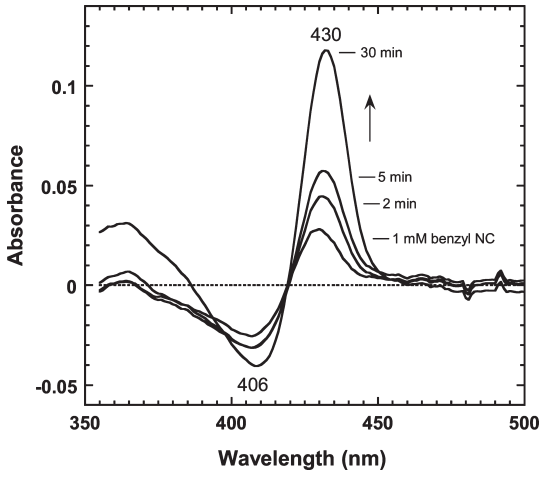

FIGURE 2: Slow equilibrium binding of benzyl isocyanide to ferric heme−CaHmx1. Shown are the absorption difference spectra of ferric heme−CaHmx1 in the presence of 1 mM benzyl isocyanide over the course of 30 min.

Equilibrium Binding of Isocyanides to the Ferrous Heme Complexes. When isocyanide is added to ferrous heme−hHO-1, the absorbance maximum shifts from 430 to 428 nm and the broad peak at 556 nm splits into peaks at 530 and 560 nm (Figure 1B). These spectral characteristics suggest a change in coordination to the heme from five-coordinate to six-coordinate in a manner analogous to isocyanide binding to myoglobin and hemoglobin (*34*). The addition of increasing concentrations of isocyanide to the ferrous heme complexes of hHO-1 and CaHmx1 resulted in an increase and blue-shift in the Soret to generate optical difference spectra with a peak at 428 nm and a trough at 441 nm. However, the binding of isocyanide to reduced CYP3A4 gives rise to a type-III optical difference spectrum (Figure 3), characterized by two pH dependent peaks in the Soret region at 430 and 450 nm (*35*) and is similar to those observed with alkylamines (SKF-525A) and arylamines (*p*-chloroaniline). Here the data were best fit to the equation for a single, high affinity binding site.

The difference in affinity ranged from 200- to 500-fold between the ferric and ferrous forms of hHO-1 (Table 1), while the difference is much less for CYP3A4. Unfortunately the high affinity of the ferrous heme−hHO-1 for isocyanides meant that the observed K_D values were well below the enzyme concentration and therefore could not be determined with sufficient accuracy by this method. Therefore we turned to kinetic methods

for a more accurate determination of the affinity for ferrous hHO-1.

Kinetic Studies of Isocyanide Binding to Ferrous Heme−hHO-1. The rate of association and dissociation for the isocyanides provides another means to obtain the equilibrium constants for binding of the isocyanides to the ferrous form of the enzyme. Binding kinetics of isocyanides to hHO-1 were investigated using absorbance measurements at different ligand concentrations. The spectra, acquired as a function of time, displayed an increase in absorbance at 428 nm and a decrease in absorbance at 441 nm (Figure 4A).

The kinetic traces extracted at 428 nm were used to estimate the rate of binding. For all the isocyanide ligands, the kinetics were fitted to single exponentials. The second-order association rate constants for binding of the isocyanides to ferrous heme−hHO-1 were obtained from the slopes of the linear plots of the observed pseudo-first-order rate constants (k_{obs}) versus ligand concentration (Figure 5). The association rate constants for isopropyl, *n*-butyl, and benzyl isocyanide to the ferrous form of heme−hHO-1 are all ~3-fold apart. The association rate constant for isopropyl isocyanide (1.3 μM^{-1} s^{-1}) is comparable to that of CO (0.9 μM^{-1} s^{-1}) (*36*), while the association rate constant for *n*-butyl isocyanide (3.9 μM^{-1} s^{-1}) is less than, but still comparable to, that of O_2 (6.9 μM^{-1} s^{-1}) (*36*). In contrast, benzyl isocyanide (k_{on} = 11.2 μM^{-1} s^{-1}) associates approximately 1.6 times faster than O_2, the next best ligand.

Dissociation kinetics were initially probed using CO as a replacement ligand. However, reactions of *n*-butyl isocyanide and benzyl isocyanide in the presence of CO either reached equilibrium at a halfway point or did not occur at all. NO was found to readily displace all of the isocyanides. Experiments were performed with a minimal amount of dithionite, to ensure fully reduced enzyme, but were maintained anaerobic by the presence of a glucose oxidase system. The spectra, acquired as a function of time, displayed an increase in absorbance at 416 nm due to NO binding to ferrous heme−hHO-1 and a decrease in absorbance at

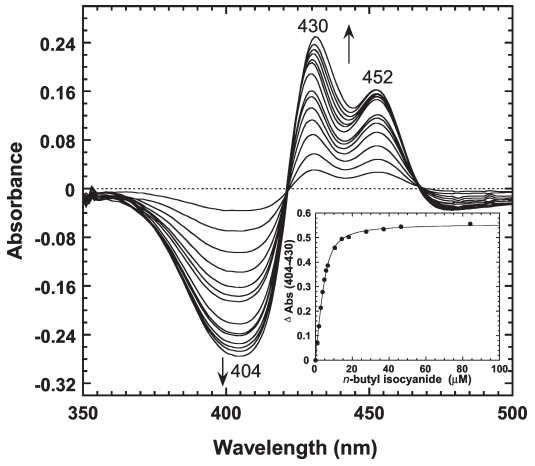

FIGURE 3: Binding of *n*-butyl isocyanide to reduced CYP3A4. Shown are type-III difference spectra of ferrous CYP3A4 in the presence of successive additions of *n*-butyl isocyanide with the resulting titration curve (inset).

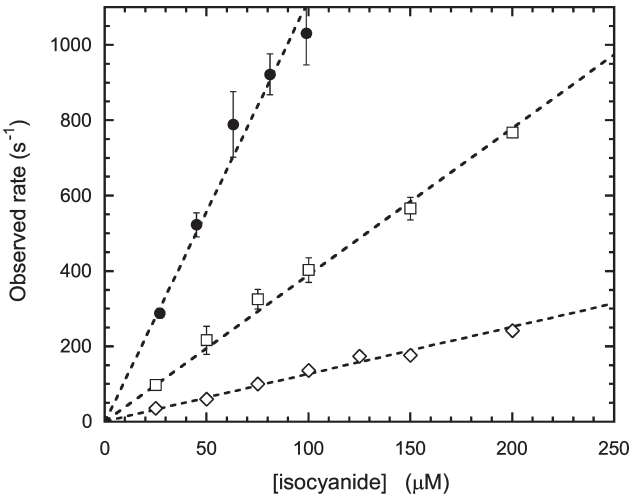

FIGURE 5: Estimation of isocyanide binding rate to ferrous heme−hHO-1. Shown are the dependence of the observed pseudo-first-order association rates on isopropyl isocyanide (◇), *n*-butyl isocyanide (□), and benzyl isocyanide (●) concentration. The data are presented as group means ± SD.

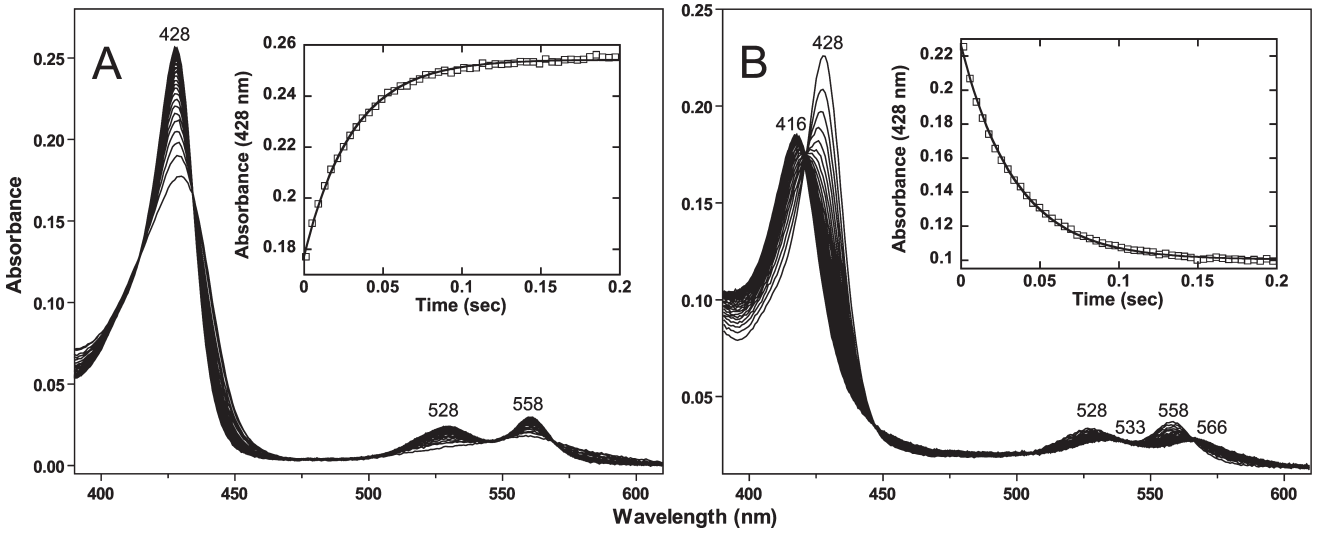

FIGURE 4: Binding kinetics of isocyanides to ferrous heme−hHO-1. (A) Binding of isopropyl isocyanide (25 μM) to ferrous heme−hHO-1 (2.5 μM) with the corresponding change in absorbance at 428 nm (inset) fitted to a single exponential. (B) Dissociation reaction of ferrous heme−hHO-1 (2.5 μM) prebound to benzyl isocyanide (5 μM) in the presence of ~1 mM NO. The change in absorbance at 428 nm (inset) was fitted to a single exponential equation. Scans are shown at every 0.4 ms.

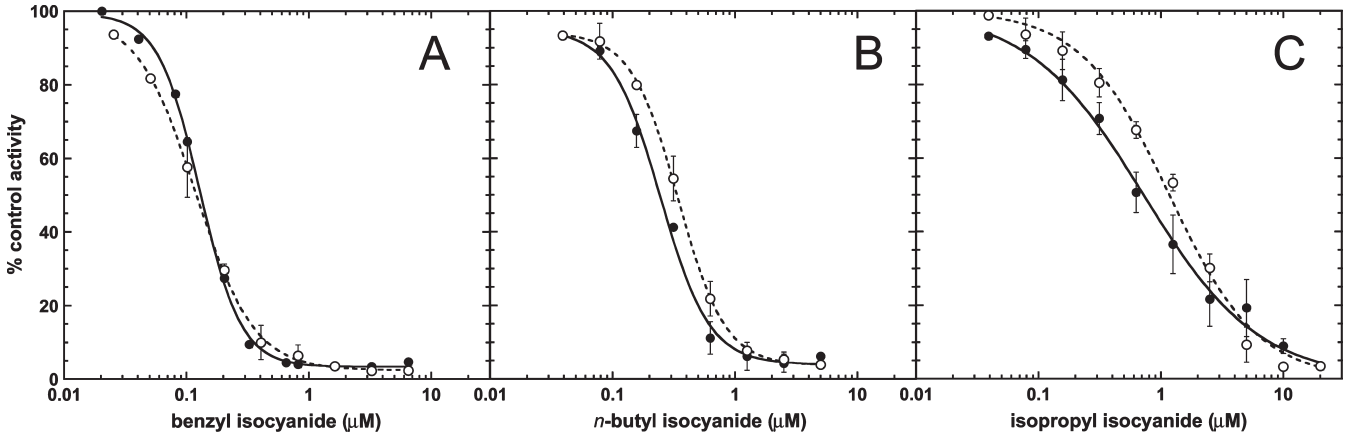

FIGURE 6: Inhibition of human heme oxygenases activity by isocyanides. Concentration−response curves for hHO-1 (●) and hHO-2 (○) isoforms were obtained in the presence of (A) benzyl isocyanide, (B) *n*-butyl isocyanide, and (C) isopropyl isocyanide. The data are presented as group means ± SD.

428 nm (Figure 4B). The rates of ligand displacement in the presence of NO were monophasic. Isopropyl ($k_{off} = 0.65\ s^{-1}$) and *n*-butyl isocyanide ($k_{off} = 0.52\ s^{-1}$) have very similar dissociation rates, while benzyl isocyanide ($k_{off} = 0.26\ s^{-1}$) is approximately half as fast, with a rate similar to that of O_2 displacement ($0.25\ s^{-1}$) (*36*).

The K_D values extracted from the association and dissociation rates resemble those measured by equilibrium titration (Table 1). Thus isopropyl and *n*-butyl isocyanide bind to the ferrous heme−hHO-1 with K_D constants of 0.52 and 0.12 μM, respectively. Only benzyl isocyanide, with a $K_D = 0.02$ μM, is competitive with O_2 ($K_D = 0.04$ μM) (*36*). However, O_2 binding to the heme is expected to be inhibited much more effectively by CO ($K_D = 0.01$ μM) (*36*) due to its very slow dissociation rate ($0.009\ s^{-1}$) (*36*).

Enzymatic Activity Assays. The IC_{50} values of the three isocyanide ligands for hHO-1 and hHO-2 were determined by varying their concentrations at a fixed heme concentration of 15 μM (Figure 6). The observed trend in inhibition matches the trend in K_D constants where the larger functional groups favor binding. The isocyanide bearing a benzyl substituent has the lowest observed IC_{50} of 0.13 ± 0.01 μM for hHO-1 and 0.10 ± 0.01 μM for hHO-2. Next is *n*-butyl isocyanide ($IC_{50}^{hHO\text{-}1} = 0.25 \pm 0.01$ μM; $IC_{50}^{hHO\text{-}2} = 0.34 \pm 0.02$ μM) with IC_{50} values 2-to 3-fold higher than benzyl isocyanide for hHO-1 and hHO-2, respectively. Finally, isopropyl isocyanide ($IC_{50}^{hHO\text{-}1} = 0.72 \pm 0.08$ μM; $IC_{50}^{hHO\text{-}2} = 1.17 \pm 0.06$ μM) has IC_{50} values 5- to 4-fold higher than butyl isocyanide for hHO-1 and hHO-2, respectively. There was no trend in selectivity observed in the inhibition of hHO-1 over hHO-2.

The inhibition kinetics of hHO-1 with benzyl isocyanide were subsequently investigated in more detail. Varying isocyanide at multiple fixed concentrations of heme characterized the type of inhibition as uncompetitive with respect to heme, showing parallel lines in the $1/v$ versus inhibitor plot (Figure 7). The ESI complex can only form after initial formation of the ES complex, supporting the idea that isocyanide is dependent upon heme binding to the enzyme active site prior to competing with O_2 for coordination to the heme iron at the distal site. However, at concentrations of benzyl isocyanide greater than 0.3 μM, the points diverge and the lines intersect due to mixed inhibition (Figure 7, inset), presumably from competitive binding of benzyl isocyanide either to free heme or to the HO heme binding pocket. Global fitting of the data (excluding the ≥0.33 μM benzyl isocyanide data) to the equation for uncompetitive binding gave the lowest error and the following kinetic parameters for hHO-1: V_{max} and K_m for heme were 35 ± 2 nmol h^{-1} $nmol^{-1}$ and 5 ± 1 μM, respectively, and K_I for benzyl isocyanide was 0.15 ± 0.02 μM. In this case, the IC_{50} value is very close to the K_I value.

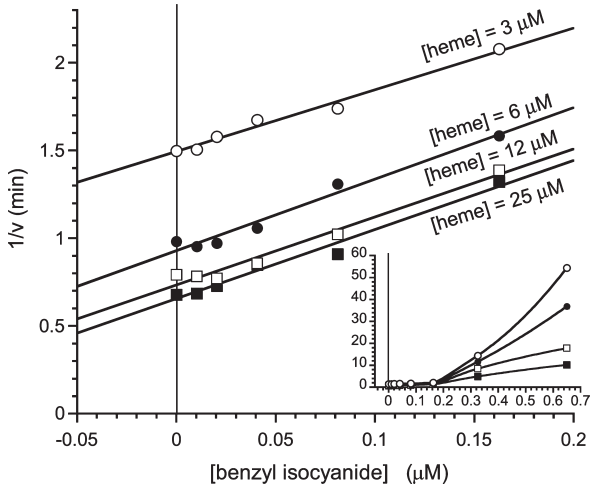

FIGURE 7: Inhibition of hHO-1 by benzyl isocyanide. Dixon plot illustrating the nonintersecting lines characteristic of uncompetitive inhibition. The concentration of heme was maintained constant, as indicated (○ = 3 μM heme; ● = 6 μM heme; □ = 12 μM heme; ■ = 25 μM heme), while the concentration of benzyl isocyanide was varied. At concentrations of inhibitor greater than 0.3 μM, the slopes are no longer equal and the lines intersect (inset).

Single-Turnover Reactions. Single-turnover experiments were performed to determine the stage of catalysis most inhibited by benzyl isocyanide on heme−hHO-1. Upon addition of NADPH and CPR, the intensity of the Soret band immediately increased and shifted to 428 nm, followed by a slow decrease. In the visible region, new bands at 530 and 558 nm, which correspond to the isocyanide coordinated ferrous heme−hHO1 complex, appeared immediately and then decreased along with the appearance of a new peak at 673 nm, corresponding to isocyanide bound ferrous verdoheme (Figure 8). The addition of CO as a ferrous heme ligand had no affect on the absorbance spectrum nor did ferricyanide, as an oxidant. Conversion of verdoheme to biliverdin was not detected spectroscopically at concentrations of isocyanide ≥10 μM (2 equivalents). Even at benzyl isocyanide concentrations <1 equiv, the verdoheme to biliverdin step was strongly inhibited (not shown).

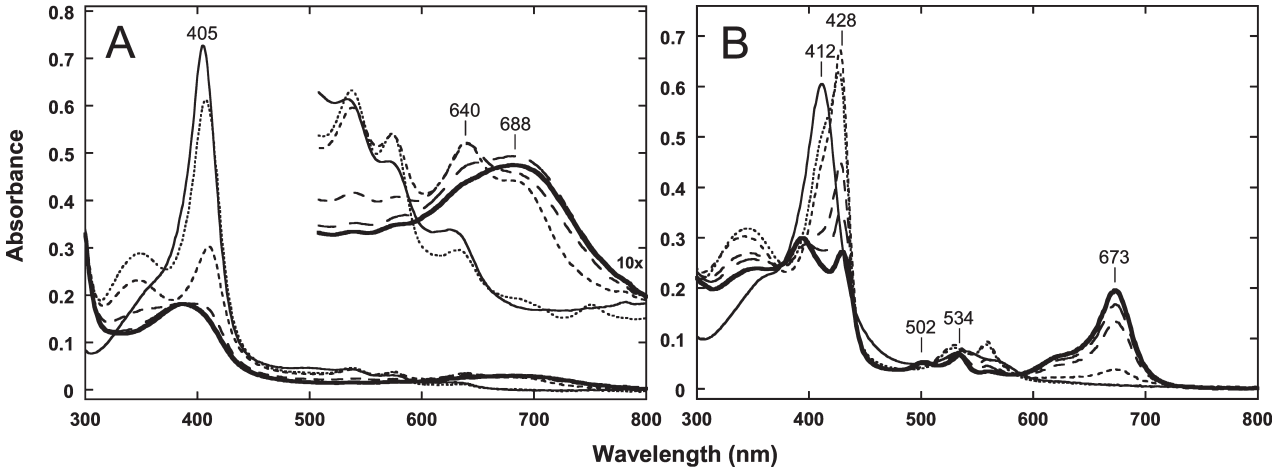

FIGURE 8: hHO catalysis inhibition at the verdoheme stage by benzyl isocyanide. Changes in the absorption spectrum during the NADPH/CPR supported single turnover reaction of 5 μM heme−hHO-1 complex in the absence (A) and in the presence of 26 μM benzyl isocyanide (B). The spectra were recorded before (solid line), and after the addition of NADPH (···), 2 (---), 5 (− − −), 10 (———), and 20 min (thick solid line).

The rate of conversion of heme to verdoheme was estimated by the initial rate of the decrease in magnitude of the Soret band. The first reaction with O_2 occurs quickly and requires significant concentrations of benzyl isocyanide ($\geq$500 μM) to effectively inhibit the reaction. Fitting the data to the Hill equation was not possible, but an estimate of the IC_{50} from the reaction was approximately 5 and 45 μM for hHO-1 in the presence of benzyl isocyanide and *n*-butyl isocyanide, respectively. Therefore the very low observed IC_{50} and K_I values are most likely due to the very tight binding of isocyanide to the verdoheme−hHO-1 form and not to the heme−hHO-1 form.

Equilibrium Binding of Isocyanides to Ferric Verdoheme−hHO-1. We evaluated the affinity of isocyanides for the ferric verdoheme of hHO-1 complex, generated from the corresponding ferric heme complex and 1 equiv of H_2O_2. Binding of isocyanide to the ferric verdoheme−hHO-1 induced a decrease and red-shift of the Soret, as observed for the ferric heme proteins. Addition of 600 μM *n*-butyl isocyanide to the ferric verdoheme−hHO-1 displaced the Soret maximum from 405 to 411 nm and bands at 535 and 676 nm emerged (Figure 9). The dissociation constants (K_D) of the isocyanides were determined according to the difference spectra and the resulting titration curves (Figure 10). Thus, the ferric verdoheme−hHO-1 shows a 2-fold higher affinity for *n*-butyl and benzyl isocyanide than ferric heme−hHO-1, with an affinity for *n*-butyl and benzyl isocyanide of 17 ± 3 and 3 ± 1.5 μM, respectively, whereas isopropyl isocyanide displayed weaker binding with a K_D equal to 440 ± 75 μM.

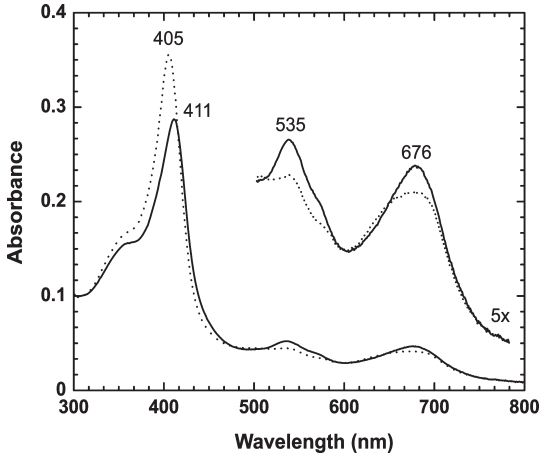

FIGURE 9: Binding of *n*-butyl isocyanide to the ferric verdoheme−hHO-1. Shown are the absorption spectra of ferric verdoheme−hHO-1 in the presence (solid line) and absence (dotted line) of 600 μM *n*-butyl isocyanide.

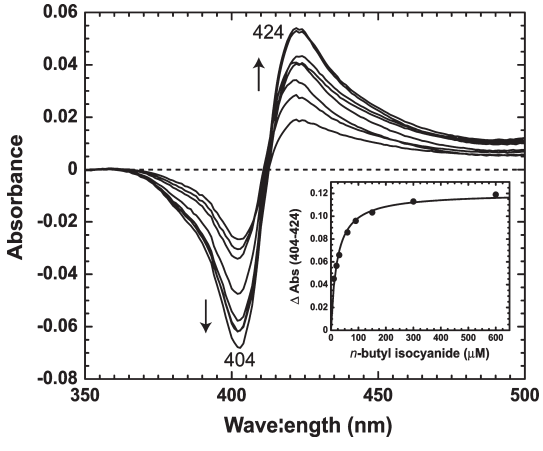

FIGURE 10: Titration of *n*-butyl isocyanide into the ferric verdoheme−hHO-1. Difference spectra of ferric verdoheme−hHO-1 in the presence of increasing concentrations of *n*-butyl isocyanide (10−600 μM) with the resulting titration curve (inset).

DISCUSSION

Strategies to specifically target heme oxygenases for therapeutic intervention could be fruitful in the treatment of variety of pathogenic infections and cancer. There are multiple strategies for inhibiting HOs. For example, nonredox active heme analogues such as Sn-heme with a K_I = 0.011 μM (*37*), bind to the HO active site very tightly via metal coordination to the distal histidine ligand and compete directly with the natural substrate but are unselective and inhibit a number of other heme dependent enzymes including cytochrome P450 (*38*), NOS (*39*), and sGC (*40*). Another HO inhibition strategy utilizes chemicals with azalanstat-like chemical structure. Azalanstat was a cytochrome P450 inhibitor containing an imidazole-dioxolane framework (*10*), effectively competing with O_2 for binding to the heme substrate within the active site. Although these chemicals are nonselective for NOS and sGC, they are potent

P450 inhibitors (*41*), the inhibition of which must be minimalized to avoid the possibility of drug−drug interactions. Another strategy has identified small-molecule inhibitors that bind to the heme free HOs from *Neisseria meningitidis* and *Pseudomonas aeruginosa* by in silico screening of a large number of compounds. Several of these inhibitors were shown to have K_D values in the low micromolar range (*42*). However, high concentrations of a weak binding inhibitor would be needed to compete directly with heme ($K_D = 0.8 \pm 0.2$ μM) (*43*). Our goal was to probe the feasibility of using isocyanides as HO inhibitors. We showed that more apolar isocyanides can bind very tightly to ferrous heme−hHO-1 and CaHmx1, with a greater than 13-fold selectivity over ferrous CYP3A4.

Precedence exists for the use of isocyanides as inhibitors of a heme dependent process. Terpene isocyanides, isolated from marine sponges, exhibit antimalarial activities by inhibiting sequestration of heme into beta hematin, presumably by coordination to the heme iron (*44*). Because of their apolar nature, isocyanides can be used as molecular probes to identify the location of apolar cavities and to explore their dimensions. For example, the primary use of isocyanides has been toward studying their equilibrium-binding properties to heme-containing proteins, such as hemoglobin and myoglobin (*15*, *16*). Isocyanide migration from the solvent into the protein is rate limiting and the overall association rate constants for the binding of these ligands are sensitive to changes in the accessibility of the heme pocket (*45*). Once the isocyanide is trapped within the protein matrix of a heme-containing protein it often results in coordination of the isocyanide carbon atom to the Fe atom of the heme group. The affinities of isocyanides for heme proteins have been shown to be strongly affected by steric hindrance between the bound ligand and nearby residues (*46*).

Our findings indicate that the large hydrophobic cavity seen in the crystal structure of hHO-1 (*47*) and hHO-2 (*48*) is able to effectively bind the more bulky hydrophobic benzyl isocyanide. The stabilizing $\pi-\pi$ interactions between the phenyl ring of the ligand and a nearby aromatic side-chain may contribute to the increased affinity, although lipophilicity may alone explain the increase. The HOs from pathogenic bacteria such as *N. meningitides* and *Corynebacterium diphtheriae* share very little sequence identity with hHO-1, but they do share the same unique α-helical fold that is characteristic of all HOs and a smaller hydrophobic cavity. *C. albicans*, a type of yeast that is commonly found inhabiting human mucous membranes, can become particularly dangerous to individuals with an impaired immune response. CaHmx1 is required for the utilization of heme as a nutritional iron source (*19*). The structure of CaHmx1 is not yet known, but the difficulties we encountered binding ligands to the ferric resting state of heme−CaHmx1 suggest a deeply buried active site that is more readily accessed by the more hydrophobic ligands. Furthermore, tight binding of benzyl isocyanide to the ferrous form suggests the presence of a similar hydrophobic cavity.

Oxidation of heme by HO occurs in a stepwise fashion, proceeding through α-*meso*-hydroxyheme and verdoheme intermediates, with dissociation of the product CO followed by Fe^{2+} and finally biliverdin. Oxidative breakdown of verdoheme to biliverdin proceeds without interference by CO (*49*), which is a byproduct of the conversion of α-*meso*-hydroxyheme to verdoheme. However, an excess amount of exogenous CO does inhibit this third step and is analogous to the mode of inhibition displayed by isocyanides and imidazole-dioxolane compounds (*12*). Among the three O_2 reactions of HO catalysis, the verdoheme−HO-1 complex has the lowest reactivity with O_2, with an estimated rate constant of 2.5×10^2 M^{-1} s^{-1} in the presence of reductant (*50*) that is over 4 orders of magnitude slower than ferrous heme−HO-1 complex binds O_2. Therefore, the verdoheme form of heme oxygenase is most susceptible to inhibition by small gaseous molecules like CO or isocyanides. Inhibition at the verdoheme stage evident in the single turnover experiments was further supported by the improved affinities of *n*-butyl and benzyl isocyanides for the ferric verdoheme−hHO-1 complex.

In conclusion, we have established for the first time the equilibrium binding of three isocyanides; isopropyl, *n*-butyl, and benzyl, to hHO-1 and hHO-2, CaHmx1, and CYP3A4. Isocyanides bound to both ferric and ferrous HO-bound heme, with higher affinity between the more hydrophobic isocyanides and significantly tighter binding to the ferrous form. Among the enzymes evaluated here, benzyl isocyanide exhibited the strongest affinity for the ferrous heme complexes. In this work, we also established the binding parameters of the isocyanides to the ferrous form of hHO-1. Here it was demonstrated unequivocally that benzyl isocyanide was a potent uncompetitive inhibitor of hHO-1, catalytic turnover being completely suppressed by isocyanide binding to the verdoheme intermediate. Thus, the mode of isocyanide inhibition is unique to HO among heme containing proteins and may support the development of more selective HO inhibitors.

REFERENCES

1. Ryter, S. W., Alam, J., and Choi, A. M. (2006) Heme oxygenase-1/carbon monoxide: from basic science to therapeutic applications. *Physiol. Rev. 86*, 583–650.
2. Kim, H. P., Ryter, S. W., and Choi, A. M. (2006) CO as a cellular signaling molecule. *Annu. Rev. Pharmacol. Toxicol. 46*, 411–449.
3. Zakhary, R., Poss, K. D., Jaffrey, S. R., Ferris, C. D., Tonegawa, S., and Snyder, S. H. (1997) Targeted gene deletion of heme oxygenase 2 reveals neural role for carbon monoxide. *Proc. Natl. Acad. Sci. U.S.A. 94*, 14848–14853.
4. Stocker, R., and Perrella, M. A. (2006) Heme oxygenase-1: a novel drug target for atherosclerotic diseases? *Circulation 114*, 2178–2189.
5. Fang, J., Akaike, T., and Maeda, H. (2004) Antiapoptotic role of heme oxygenase (HO) and the potential of HO as a target in anticancer treatment. *Apoptosis 9*, 27–35.
6. Skaar, E. P., Humayun, M., Bae, T., DeBord, K. L., and Schneewind, O. (2004) Iron-source preference of *Staphylococcus aureus* infections. *Science 305*, 1626–1628.
7. Vreman, H. J., Cipkala, D. A., and Stevenson, D. K. (1996) Characterization of porphyrin heme oxygenase inhibitors. *Can. J. Physiol. Pharmacol. 74*, 278–285.
8. Grundemar, L., and Ny, L. (1997) Pitfalls using metalloporphyrins in carbon monoxide research. *Trends Pharmacol. Sci. 18*, 193–195.
9. Sahoo, S. K., Sawa, T., Fang, J., Tanaka, S., Miyamoto, Y., Akaike, T., and Maeda, H. (2002) Pegylated zinc protoporphyrin: a water-soluble heme oxygenase inhibitor with tumor-targeting capacity. *Bioconjugate Chem. 13*, 1031–1038.
10. Vlahakis, J. Z., Kinobe, R. T., Bowers, R. J., Brien, J. F., Nakatsu, K., and Szarek, W. A. (2005) Synthesis and evaluation of azalanstat analogues as heme oxygenase inhibitors. *Bioorg. Med. Chem. Lett. 15*, 1457–1461.
11. Roman, G., Riley, J. G., Vlahakis, J. Z., Kinobe, R. T., Brien, J. F., Nakatsu, K., and Szarek, W. A. (2007) Heme oxygenase inhibition by 2-oxy-substituted 1-(1*H*-imidazol-1-yl)-4-phenylbutanes: effect of halogen substitution in the phenyl ring. *Bioorg. Med. Chem. 15*, 3225–3234.
12. Sugishima, M., Higashimoto, Y., Oishi, T., Takahashi, H., Sakamoto, H., Noguchi, M., and Fukuyama, K. (2007) X-ray crystallographic and biochemical characterization of the inhibitory action of an imidazole-dioxolane compound on heme oxygenase. *Biochemistry 46*, 1860–1867.
13. Rahman, M. N., Vlahakis, J. Z., Szarek, W. A., Nakatsu, K., and Jia, Z. (2008) X-ray crystal structure of human heme oxygenase-1 in complex with 1-(adamantan-1-yl)-2-(1*H*-imidazol-1-yl)ethanone:

a common binding mode for imidazole-based heme oxygenase-1 inhibitors. *J. Med. Chem. 51*, 5943–5952.
14. Sugishima, M., Sakamoto, H., Noguchi, M., and Fukuyama, K. (2004) CO-trapping site in heme oxygenase revealed by photolysis of its CO-bound heme complex: Mechanism of escaping from product inhibition. *J. Mol. Biol. 341*, 7–13.
15. Reisberg, P. I., and Olson, J. S. (1980) Equilibrium binding of alkyl isocyanides to human hemoglobin. *J. Biol. Chem. 255*, 4144–4130.
16. Mims, M. P., Porras, A. G., Olson, J. S., Noble, R. W., and Peterson, J. A. (1983) Ligand binding to heme proteins. An evaluation of distal effects. *J. Biol. Chem. 258*, 14219–14232.
17. Yoneyama, H., Hori, H., and Ichikawa, Y. (1997) Optical and electron paramagnetic resonance absorption spectra of complexes of nitric oxide synthase I with isocyanides. *Biochim. Biophys. Acta 1335*, 253–264.
18. Imai, Y., Okamoto, N., Nakahara, K., and Shoun, H. (1997) Absorption spectral studies on heme ligand interactions of P-450nor. *Biochim. Biophys. Acta 1337*, 66–74.
19. Santos, R., Buisson, N., Knight, S., Dancis, A., Camadro, J. M., and Lesuisse, E. (2003) Haemin uptake and use as an iron source by *Candida albicans*: role of CaHMX1-encoded haem oxygenase. *Microbiology 149*, 579–588.
20. Guengerich, F. P. (1988) Oxidation of 17 alpha-ethynylestradiol by human liver cytochrome P-450. *Mol. Pharmacol. 33*, 500–508.
21. Wrighton, S. A., and Stevens, J. C. (1992) The human hepatic cytochromes P450 involved in drug metabolism. *Crit. Rev. Toxicol. 22*, 1–21.
22. Hildebrandt, A. G., Roots, I., Tjoe, M., and Heinemeyer, G. (1978) Hydrogen peroxide in hepatic microsomes. *Methods Enzymol. 52*, 342–350.
23. Wilks, A., Black, S. M., Miller, W. L., and Ortiz de Montellano, P. R. (1995) Expression and characterization of truncated human heme oxygenase (hHO-1) and a fusion protein of hHO-1 with human cytochrome P450 reductase. *Biochemistry 34*, 4421–4427.
24. Lightning, L. K., Huang, H., Moenne-Loccoz, P., Loehr, T. M., Schuller, D. J., Poulos, T. L., and Ortiz de Montellano, P. R. (2001) Disruption of an active site hydrogen bond converts human heme oxygenase-1 into a peroxidase. *J. Biol. Chem. 276*, 10612–10619.
25. Dierks, E. A., Davis, S. C., and Ortiz de Montellano, P. R. (1998) Glu-320 and Asp-323 are determinants of the CYP4A1 hydroxylation regiospecificity and resistance to inactivation by 1-aminobenzotriazole. *Biochemistry 37*, 1839–1847.
26. Kim, D., Yukl, E. T., Moenne-Loccoz, P., and Montellano, P. R. (2006) Fungal heme oxygenases: Functional expression and characterization of Hmx1 from *Saccharomyces cerevisiae* and CaHmx1 from *Candida albicans*. *Biochemistry 45*, 14772–14780.
27. Gillam, E. M., Baba, T., Kim, B. R., Ohmori, S., and Guengerich, F. P. (1993) Expression of modified human cytochrome P450 3A4 in *Escherichia coli* and purification and reconstitution of the enzyme. *Arch. Biochem. Biophys. 305*, 123–131.
28. Liu, Y., Moenne-Loccoz, P., Loehr, T. M., and Ortiz de Montellano, P. R. (1997) Heme oxygenase-1, intermediates in verdoheme formation and the requirement for reduction equivalents. *J. Biol. Chem. 272*, 6909–6917.
29. Wilks, A., and Ortiz de Montellano, P. R. (1993) Rat liver heme oxygenase. High level expression of a truncated soluble form and nature of the meso-hydroxylating species. *J. Biol. Chem. 268*, 22357–22362.
30. Yoshida, T., and Kikuchi, G. (1978) Purification and properties of heme oxygenase from pig spleen microsomes. *J. Biol. Chem. 253*, 4224–4229.
31. Takahashi, S., Wang, J., Rousseau, D. L., Ishikawa, K., Yoshida, T., Host, J. R., and Ikeda-Saito, M. (1994) Heme−heme oxygenase complex. Structure of the catalytic site and its implication for oxygen activation. *J. Biol. Chem. 269*, 1010–1014.
32. Yano, J. K., Wester, M. R., Schoch, G. A., Griffin, K. J., Stout, C. D., and Johnson, E. F. (2004) The structure of human microsomal cytochrome P450 3A4 determined by X-ray crystallography to 2.05-A resolution. *J. Biol. Chem. 279*, 38091–38094.
33. Williams, P. A., Cosme, J., Vinkovic, D. M., Ward, A., Angove, H. C., Day, P. J., Vonrhein, C., Tickle, I. J., and Jhoti, H. (2004) Crystal structures of human cytochrome P450 3A4 bound to metyrapone and progesterone. *Science 305*, 683–686.
34. Derbyshire, E. R., and Marletta, M. A. (2007) Butyl isocyanide as a probe of the activation mechanism of soluble guanylate cyclase. Investigating the role of non-heme nitric oxide. *J. Biol. Chem. 282*, 35741–35748.
35. Beumel, G. A., Levi, P. E., and Hodgson, E. (1985) Spectral interactions of piperonyl butoxide and isocyanides with purified hepatic cytochrome P-450 from uninduced mice. *Gen. Pharmacol. 16*, 193–197.
36. Migita, C. T., Matera, K. M., Ikeda-Saito, M., Olson, J. S., Fujii, H., Yoshimura, T., Zhou, H., and Yoshida, T. (1998) The oxygen and carbon monoxide reactions of heme oxygenase. *J. Biol. Chem. 273*, 945–949.
37. Drummond, G. S., and Kappas, A. (1981) Prevention of neonatal hyperbilirubinemia by tin protoporphyrin IX, a potent competitive inhibitor of heme oxidation. *Proc. Natl. Acad. Sci. U.S.A. 78*, 6466–6470.
38. Trakshel, G. M., Sluss, P. M., and Maines, M. D. (1992) Comparative effects of tin- and zinc-protoporphyrin on steroidogenesis: tin-protoporphyrin is a potent inhibitor of cytochrome P-450-dependent activities in the rat adrenals. *Pediatr. Res. 31*, 196–201.
39. Luo, D., and Vincent, S. R. (1994) Metalloporphyrins inhibit nitric oxide-dependent cGMP formation in vivo. *Eur. J. Pharmacol. 267*, 263–267.
40. Glaum, S. R., and Miller, R. J. (1993) Zinc protoporphyrin-IX blocks the effects of metabotropic glutamate receptor activation in the rat nucleus tractus solitarii. *Mol. Pharmacol. 43*, 965–969.
41. Kinobe, R. T., Vlahakis, J. Z., Vreman, H. J., Stevenson, D. K., Brien, J. F., Szarek, W. A., and Nakatsu, K. (2006) Selectivity of imidazole-dioxolane compounds for in vitro inhibition of microsomal haem oxygenase isoforms. *Br. J. Pharmacol. 147*, 307–315.
42. Furci, L. M., Lopes, P., Eakanunkul, S., Zhong, S., MacKerell, A. D. Jr., and Wilks, A. (2007) Inhibition of the bacterial heme oxygenases from *Pseudomonas aeruginosa* and *Neisseria meningitidis*: novel antimicrobial targets. *J. Med. Chem. 50*, 3804–3813.
43. Wilks, A., Ortiz de Montellano, P. R., Sun, J., and Loehr, T. M. (1996) Heme oxygenase (HO-1): His-132 stabilizes a distal water ligand and assists catalysis. *Biochemistry 35*, 930–936.
44. Wright, A. D., Wang, H., Gurrath, M., Konig, G. M., Kocak, G., Neumann, G., Loria, P., Foley, M., and Tilley, L. (2001) Inhibition of heme detoxification processes underlies the antimalarial activity of terpene isonitrile compounds from marine sponges. *J. Med. Chem. 44*, 873–885.
45. Gibson, Q. H., Olson, J. S., McKinnie, R. E., and Rohlfs, R. J. (1986) A kinetic description of ligand binding to sperm whale myoglobin. *J. Biol. Chem. 261*, 10228–10239.
46. Rohlfs, R. J., Mathews, A. J., Carver, T. E., Olson, J. S., Springer, B. A., Egeberg, K. D., and Sligar, S. G. (1990) The effects of amino acid substitution at position E7 (residue 64) on the kinetics of ligand binding to sperm whale myoglobin. *J. Biol. Chem. 265*, 3168–3176.
47. Lad, L., Schuller, D. J., Shimizu, H., Friedman, J., Li, H., Ortiz de Montellano, P. R., and Poulos, T. L. (2003) Comparison of the heme-free and -bound crystal structures of human heme oxygenase-1. *J. Biol. Chem. 278*, 7834–7843.
48. Bianchetti, C. M., Yi, L., Ragsdale, S. W., and Phillips, G. N.Jr. (2007) Comparison of apo- and heme-bound crystal structures of a truncated human heme oxygenase-2. *J. Biol. Chem. 282*, 37624–37631.
49. Liu, Y., and Ortiz de Montellano, P. R. (2000) Reaction intermediates and single turnover rate constants for the oxidation of heme by human heme oxygenase-1. *J. Biol. Chem. 275*, 5297–5307.
50. Matsui, T., Nakajima, A., Fujii, H., Matera, K. M., Migita, C. T., Yoshida, T., and Ikeda-Saito, M. (2005) O(2)- and H(2)O(2)-dependent verdoheme degradation by heme oxygenase: reaction mechanisms and potential physiological roles of the dual pathway degradation. *J. Biol. Chem. 280*, 36833–36840.